Accepted Manuscript

Title: MCR-1: a promising target for structure-based design of inhibitors to tackle polymyxin resistance

Authors: Soo Jung Son, Renjie Huang, Christopher J. Squire, Ivanhoe K.H. Leung

PII: S1359-6446(18)30025-4
DOI: https://doi.org/10.1016/j.drudis.2018.07.004
Reference: DRUDIS 2287

To appear in:

Please cite this article as: Son, Soo Jung, Huang, Renjie, Squire, Christopher J., Leung, Ivanhoe K.H., MCR-1: a promising target for structure-based design of inhibitors to tackle polymyxin resistance.Drug Discovery Today https://doi.org/10.1016/j.drudis.2018.07.004

MCR-1: a promising target for structure-based design of inhibitors to tackle polymyxin resistance

Soo Jung Son,[1] Renjie Huang,[1] Christopher J. Squire,[2,3] and Ivanhoe K.H. Leung[1]

[1]School of Chemical Sciences, The University of Auckland, Victoria Street West, Private Bag 92019, Auckland 1142, New Zealand
[2]School of Biological Sciences, The University of Auckland, Victoria Street West, Private Bag 92019, Auckland 1142, New Zealand
[3]Maurice Wilkins Centre for Molecular Biodiscovery, c/o The University of Auckland, Victoria Street West, Private Bag 92019, Auckland 1142, New Zealand
Corresponding authors: Son, S.J. (aimee.son@auckland.ac.nz); Squire, C.J. (c.squire@auckland.ac.nz); Leung, I.K.H. (i.leung@auckland.ac.nz)

Highlights

- MCR-1 is a phosphoethanolamine transferase that causes polymyxin resistance, an alarming worldwide antibiotic resistance threat
- Zinc ions are critical for MCR-1 function but the number of biologically relevant zinc sites is not well defined
- A two-step mechanism of MCR-1 action transfers phosphoethanolamine to lipid A, modifying the bacterial surface charge and rendering polymyxins ineffective
- MCR1 crystal structures provide starting points for rational drug discovery efforts

Keywords: MCR-1; polymyxin antibiotic resistance; enzymatic mechanism; phosphoethanolamine transferase; integral membrane protein; zinc metalloprotein.
Teaser: The structure and enzymatic mechanism of MCR-1 drive drug discovery efforts towards combating the rising worldwide threat of resistance to last-resort polymyxin antibiotics.

The spread of a novel mobile colistin resistance gene (*mcr1*) has jeopardised the use of polymyxins, last-resort antibiotics that are used increasingly to treat infections caused by multidrug-resistant (MDR) Gram-negative pathogens. In early 2017, the WHO reported the global spread of *mcr1* within a few years after its initial discovery in China. The protein encoded by *mcr1* is a putative 60-kDa phosphoethanolamine (pEtN) transferase, MCR-1, and has been studied extensively since its discovery. Herein, we present a comprehensive review of MCR-1 covering its structure, function, and mechanism, to call for the rational drug design of molecular inhibitors of MCR-1 to use in colistin-based combination therapies.

Introduction

Among the various classes of modern antibiotic, the polymyxins are a structurally distinct class of nonribosomal, cyclic peptides that are used as the 'last line' of defence against MDR Gram-negative pathogens. Polymyxins use is associated with extensive neuro- and nephrotoxicity, but is fuelled by a lack of breakthrough research in developing novel antibiotics to treat MDR bacterial infections [1]. One of the best known polymyxins, colistin or polymyxin E, is typically used in the treatment of carbapenemase-producing *Enterobacteriaceae*, bacterial isolates that have acquired resistance against almost all antibiotics, including carbapenems. Although bacterial resistance to colistin was previously considered rare, increasing drug consumption and contemporary medical practices have resulted in lipid A-mediated chromosomal resistance mutations becoming more commonplace, with reports of resistance emerging from 2012 onwards [2–4].

In 2015, plasmid-borne colistin resistance was first reported and shown to spread and diverge easily and rapidly between different bacterial populations [5]. In this report in *Lancet Infectious Disease,* Liu and colleagues identified a novel mobile colistin resistance gene (*mcr1*) isolated from *Escherichia coli* found in raw meat, animal, and human samples in China [5]. This transmissible colistin resistance conferred by *mcr1* was also significant, given that the colistin-resistance bacteria could apparently spread via the food chain [6]. *Mcr1* was confined to China at the time of the first report, but as of February 2017, the gene had been detected in more than 30 countries on five continents, posing a serious escalation of the current antibiotic resistance crisis [7]. More recently, genetic variants of *mcr1* have been reported, namely *mcr2*, *mcr3*, *mcr4*, and *mcr5,* underscoring the on-going evolution of the mobile colistin resistance [8–10].

Mcr1 encodes a 60.1-kDa (541 amino acid) cytoplasmic transmembrane protein known as MCR-1, which is found in Gram-negative bacteria. Multiple sequence alignment predicted the protein to be a pEtN transferase, and this was recently confirmed by both *in vitro* and *in vivo* experiments where MCR-1 was shown to attach a pEtN moiety to the lipid A head groups of lipopolysaccharide (LPS), one of the major constituents of the Gram-negative bacterial membrane [11]. Such modification of the 1′ or 4′ location of the lipid A head group has the effect of concealing negatively charged phosphate groups on the bacterial surface and abolishing the initial electrostatic attraction that colistin and other polymyxin drugs heavily rely on (Figure 1).

The absolute number of severe cases worldwide requiring colistin treatment is substantial because of the high frequency of infections resulting from *Enterobacteraceae* [6]. Consequently, in response to the emergence and alarming spread of *mcr1*, the WHO has classified polymyxins as one of the 'Highest Priority Critically Important Antimicrobials' to ensure more prudent and rational use of the drugs [6]. There is a pressing need for inhibition of MCR-1 as a mode of prolonging the usefulness of polymyxin antibiotics and enhancing innate immune clearance.

In this review, we present recent landmark discoveries around the structure and function of MCR-1, and provide mechanistic insights with the aim of stimulating more extensive investigations into the mechanism of action and inhibition of the protein. We hope that this review will inspire wider drug discovery efforts to afford new antibiotic agents that help reverse bacterial polymyxin resistance.

Polymyxins: antibacterial mechanism and pEtN transferase-mediated resistance

Colistin (polymyxin E) and polymyxin B are two clinically used antibiotics for the last-resort treatment of infections caused by MDR Gram-negative bacteria. Collectively, polymyxins belong to the family of cationic antimicrobial peptides (CAMPs) that share the same unique mechanism of action afforded by two structural features: (i) a hydrophilic cyclic polypeptide 'head' group comprising seven amino acid residues; and (ii) a long hydrophobic lipid tail that extends from the head group via three amino acids [12–14]. Of the ten amino acids comprising polymyxins, six are L-α,γ-diaminobutyric acid (L-DAB) residues that are concentrated in the head group to provide multiple positive charges at physiological pH [15].

Although the details of polymyxin function are unclear, it is generally believed that membrane lysis is one of the key pathways [15]. The primary driving force for the drug–membrane interaction is thought to be an electrostatic attraction between the cationic polymyxin head group and the anionic phosphate group of lipid A [16]. Once bound to lipid A, the lipidic tail of polymyxin penetrates the outer membrane, resulting in membrane destabilisation and increased membrane permeability [14,17]. Consequently, some polymyxins cross the outer membrane and also destroy the physical integrity of the inner bacterial membrane to promote cell lysis and death [18,19].

Several bacterial modifications of lipid A have been implicated in lipid A-mediated polymyxin resistance, including the addition of: (i) pEtN to 1′ (or 4′)-phosphate position; (ii) L-aminoarabinose (L-Ara4N) to 1′ (or 4′)-phosphate position; and (iii) glycine to a 3′-linked secondary acyl chain [20–23]. The end result of any of these modifications is the neutralisation of the negatively charged lipid A, eliminating the electrostatic attraction that dictates the initial binding of polymyxin to lipid A.

MCR-1 functions as a pEtN transferase in *Escherichia coli*

pEtN transferases provide advantages in pathogenesis in several bacteria [24]. One such example is the pilin phospho-form transferase A (PptA) protein in *Neisseria gonorrhoeae*. As part of the invasive strategy of this bacterium, this protein catalyses additions of both pEtN and phosphocholine to serine residues of the pilin subunit PilE, promoting its interactions with host proteins [25–27]. MCR-1, a putative lipid A pEtN transferase, modifies bacterial cell surface structures through the attachment of pEtN moieties. Such modification confers protection against innate immune antimicrobial peptides, such as human and avian ß-defensins, although the exact mechanism concerned remains uncharacterised [24,27–29]. Other functional characteristics of MCR-1 as a lipid A pEtN

transferase, including substrate specificity, are yet to be determined. It is also unclear whether acquisition of *mcr1* offers extra benefit to the bacterium other than polymyxin resistance. The acquisition of such additional pEtN transferase activity might disturb the surface charge balance in the outer membrane, with unknown consequences for bacterial physiology, but which might include impairment of membrane functionality.

There is growing evidence of the pEtN transferase activity of MCR-1 in *Escherichia coli* as catalysing the addition of pEtN to either the 1′ or 4′-phosphate of lipid A. In the *in vitro* experiment conducted by Xu *et al.*, purified, full-length MCR-1 was incubated with a natural substrate mimetic, nitrobenzodiazole-labelled glycerol-3-pEtN (NBD-glycerol-3-pEtN) for 20 h at room temperature [11]. The separation of the incubated mixtures using thin layer chromatography (TLC) showed that MCR-1 removed pEtN from NBD-glycerol-3-pEtN, producing NBD-glycerol.

Further experiments by this group showed pEtN transferase activity *in vivo* using a strain of *E. coli* bearing a plasmid expressing full-length MCR-1. In these experiments, the lipid A component was extracted and analysed by mass spectrometry (MS). In a control plasmid sample, a single charge state at m/z = 1797.356 was seen and corresponded to unmodified lipid A. By contrast, lipid A from the *mcr1*-positive strain showed two charge state species, one at m/z = 1797.416 and the other at 1920.501, corresponding to a mixture of unmodified and pEtN-modified molecules respectively [11].

A complete picture of the MCR-1 catalytic mechanism is not afforded by any direct experimental studies. However, multiple sequence and crystal structure alignments show characteristics of the alkaline phosphatase superfamily, and suggest a two-step enzymatic mechanism [30–32]. In the proposed mechanism, the substrate phosphatidylethanolamine (PE) first binds to MCR-1 and donates pEtN to form an MCR-1/pEtN complex. In the second step, the complex binds to Kdo2-lipid A, the most abundant lipid A species in *E. coli*, and transfers pEtN to either the 1′ or 4′-phosphate position of lipid A to neutralise the surrounding negative charges (Figure 2) [11].

The same functional mechanism is proposed in the two closest structural homologues of MCR-1, lipid A pEtN transferase A from *Neisseria meningitidis* (*Nm*EptA) and pEtN transferase C from *Campylobacter jejuni* (*Cj*EptC), all of which add pEtN to lipid A of LPS [11,21,22,33–35].

Overview of MCR-1 structure: characteristics and structural homologues

MCR-1 is a type member of the pEtN transferase family along with its structural homologues, *Nm*EptA and *Cj*EptC, with which it shares ~40% sequence identity [36]. The phylogenetic relationships of these homologues and other pEtN transferases are well described by Stogios *et al.* [37]. MCR-1 comprises two distinct domains, an N-terminal transmembrane domain constructed of five putative α-helices, and a soluble C-terminal α/ß/α sandwich domain that faces the periplasmic space (Figure 3). At present, no full structure of MCR-1 is available, although the structure of the soluble C-terminal domain has been extensively studied by X-ray crystallography, with nine structures currently deposited in the Protein Data Bank (PDB). The soluble domain structures are superimposable with one another, with only some small differences in the active site and mobile loop regions. Homology modelling studies [XX] using a full-length *Nm*EptA crystal structure, predicted that the two MCR-1 domains are connected by an extended periplasmic loop and bridging helix (BH).

The soluble periplasmic domain of MCR-1 is hemispherical in shape and adopts an α/ß/α topology comprising a centrally located seven-stranded ß-sheet decorated with eight main α-helices (Figure 3C) [32,38]. This same ß-sheet topology is also observed in the homologues, *Nm*EptA and *Cj*EptC. Some conformational variability between the homologue proteins is seen in the loops adjacent to the active site and in their C-terminal fragments, which might reflect the accommodation of different substrates that are enzyme specific [36]. Indeed, *Nm*EptA specifically transfers pEtN to only lipid A phosphoryl groups [39], whereas *Cj*EptC shows broader substrate tolerance [27,28,33]. However, the substrate preference of MCR-1 remains unclear. K348-R365 (located between S4 and H5, Figure 3A) forms a flexible loop at the active site of MCR-1 and displays an open conformation, which might indicate an open substrate entry channel (red arrow, Figure 3B) [36]. The soluble domain of MCR-1 also features several ß-α-ß-α motifs and three disulfide linkages between C281/C291, C356/C364, and C414/C422. With the exception of the C356/C364 pair, the other two disulfides are both sequentially and structurally conserved in *Nm*EptA and *Cj*EptC, which contain five and three disulfide pairs, respectively [36]. The conserved C281/C291 disulfide anchors the H2 helix (T285-M292) to the central ß-sheet to form part of the active site, whereas C414/C422 contributes to the stabilisation of a loop between K409-E423 that links S5 to H6 (Figure 3A).

The active site of MCR-1 is located within the soluble domain and centres on the highly conserved T285 residue that is found in all pEtN transferases and that acts as a catalytic nucleophile in substrate modification. The active site appears as a pocket in the centre of a large, slightly concave membrane interacting surface that has a distinct pattern of hydrophobic and charged residues (Figure 3D). The active site is coordinated by a zinc ion that is essential for function, as evidenced by abrogated minimal concentration inhibition (MIC) activity in the presence of ethylenediaminetetraacetic acid (EDTA) that has stripped the metals from the protein [31]. Variable numbers of zinc ions are observed within the active site in different crystal structures, ranging in number from one to four, although the physiologically relevant number is yet to be confirmed. A small cavity adjacent to the most conserved zinc site (labelled Zn1 in all discussions below) and the nucleophile residue T285, provides a distinct electronegative potential to attract and bind the $-NH_3^+$ moiety of the substrate pEtN (Figure 3D). Another cavity also in close proximity to the active site appears in X-ray crystal structures to accommodate a range of ligands, including D-sorbitol, glycerol, and D-glucose. This location is proposed as a lipid A-binding pocket [40]. Further in-depth discussion of the soluble domain and the features mentioned briefly above, are presented below.

The lack of a full-length crystal structure of MCR-1 has necessitated the modelling of the MCR-1 transmembrane structure and a detailed comparative analysis with the full-length homologue *Nm*EptA structure [11,41]. The first report of a full-length *Nm*EptA structure by Anandan *et al.* showed that the five α-helices of the transmembrane domain are positioned roughly parallel to each other in the cytoplasmic membrane (TMH1–TMH5, Figure 3) [41]. A structural similarity in the transmembrane domains of *Nm*EptA and MCR-1 is suggested by sequence comparison and TM helix prediction and allowed the modelling study performed by Xu *et al.* [11]. In both proteins, four of the five TM helices appear shorter than the typical width of a membrane bilayer at 30 Å (TMH1–TMH4, Figure 3). The fifth helix (TMH5, Figure 3), furthest from the N terminus and measuring ~35 Å long, transverses the entire bilayer, reaching through to the inner (cytoplasmic) membrane surface. As with other integral membrane proteins, the bordering end of the helix is decorated with an array of positively charged residues that are likely to interact with the phospholipid head group of the bilayer [42].

The overall significance of the transmembrane domain is to provide stabilisation and the correct orientation of the protein in the bilayer and is likely to be enhanced by a series of aromatic residues, such as tryptophan, tyrosine, and histidine, layering at the periplasmic membrane surface. MCR-1 loses functionality as a pEtN transferase without its transmembrane domain, emphasising its importance for the correct binding and orientation of the lipid substrates, PE and lipid A [43].

The MCR-1 active site

The active site of MCR-1 is located within the soluble periplasmic domain of the protein and could be the target of first choice for the development of molecular inhibitors. It is located at the N terminus of the H2 helix (Figure 3A) in a shallow surface depression that interacts with the transmembrane domain anchored in the inner cytoplasmic membrane [31]. The active site contains a concentration of metal-binding residues that coordinate zinc ions [40]. To date, eight crystal structures of the soluble domain are available in the PDB, which reveal different structural states of the active site [31,32,36,38,40].

Zinc binding and the T285 nucleophile: nonphosphorylated (T285) versus phosphorylated (pT285)

The active site of MCR-1 contains the highly conserved threonine residue (T285) that acts as a catalytic nucleophile and is putatively phosphorylated by pEtN; phosphorylated crystal structures (pT285) produced spontaneously in recombinant bacterial expression provide models of this intermediate or activated form of the protein structure. The active site can accommodate between one and four zinc ions, although not all might be biologically relevant and required for MCR-1 function [31,32,36,38,40].

Several crystal structures contain two zinc ions when T285 retains its native state (i.e., nonphosphorylated). The two zinc ions, Zn1 and Zn2, are held by six residues, namely E246, T285, H395, D465, H466, and H478 (an additional E300 residue from a symmetry-related molecule also contacts Zn2 in crystal structures) [31,32,36,38,40]. These six residues are conserved in the homologue EptC and EptA sequences, indicating their importance in protein function [36]. The symmetry-related E300 interaction, and the MCR-1 structures annotated as dimeric, appear to be artefacts of crystallisation and we contend are not biologically relevant. The structures by Hinchliffe *et al.* and Ma *et al.* (PDB code: 5LRM and 5GRR) show the first zinc ion is located deeper in the pocket (Zn1) and is coordinated by the side chains of T285, H466, D465, and E246 residues, whereas the second Zn (Zn2) is coordinated by the side chains of H478 and H395 (Figure 4) [31,36].

The active site structure of MCR-1 containing phosphorylated T285 (pT285) is captured in six different crystal structures, four of which (PDB codes: 5LRN, 5YLC, 5YLE, and 5YLF) show coordination of a single zinc ion (Zn1), whereas the remaining two show coordination of four zinc ions (PDB codes: 5K4P and 5GOV) [31,32,36,38,40]. The crystallisation conditions for the latter two crystal structures contain a high concentration of zinc (i.e., 200 mM).

The structure by Hinchliffe *et al.* (PDB code: 5LRN) and those by Wei *et al.* (PDB codes: 5YLC, 5YLE, and 5YLF) display a single zinc ion coordinated by the side chains of H466, E246, D465, and pT285 in a tetrahedral geometry. The side chains of H478 and H395, which were previously coordinated to the second zinc ion in the active site with the native T285, are now coordinated to the phosphate of pT285 (Figure 4B) [31,40].

By contrast, 5K4P, from Stojanoski *et al.*, shows four zinc ions surrounding pT285 in the active site, encased by an extensive network of hydrogen bonding involving ten water molecules. Zn1 coordinates the side chains of H466, E246, D465, and T285 in a tetrahedral configuration that is also seen in the pT285 active site structure containing a single zinc ion. A second zinc coordinates the side chains of H395, T285, and three water molecules in a trigonal bipyramidal geometry. The third zinc coordinates four water molecules, but no protein residues directly; two of the coordinated water molecules also share coordination with two other zinc ions. The final zinc coordinates the side chains of T285, H478, and also E405 from a symmetry-related molecule, forming bridging crystal contacts (Figure 4C) [32]. 5GOV, from Hu *et al.*, also displays this same active site coordinated by four zinc ions, with only minor differences, primarily in solvation patterns, compared with 5K4P.

Overall, only Zn1 is preserved across the multiple structures of the MCR-1 active site. The additional zinc ions observed in crystal structures, in particular those involved in interactions with symmetry-related molecules (crystal packing), are likely artefacts of high zinc concentrations in crystallisation solutions and not biologically relevant. The Zn1 cation site is present in the crystal structure of full-length *Nm*EptA as the sole zinc ion present in its active site.

Key substrate analogue: ethanolamine

The inability to capture a pEtN-T285 adduct crystallographically to date is explained by Wei *et al.* by the absence of the second substrate lipid A in complex [40]. In this situation, they suggest that the existing phosphoester bond between the phosphate group and the ethanolamine (EtN) moiety undergoes spontaneous hydrolysis and is lost, rather than forming a new phosphoester linkage with lipid A.

The pT285 species that has been trapped in crystal structures has been proposed as an intermediate state along the catalytic pathway of pEtN transfer by MCR-1. However, it is also possible that pT285 is simply a nonbiologically relevant modification forced during recombinant overexpression of an incomplete, partial form of the protein at high concentration (and not membrane bound). This phosphorylation of T285 might instead validate the inherent reactive potential of this residue (and the active site) towards phosphorylation (by PE). As such, the pT285 structures, in particular in combination with the EtN binding observed in the 5YLE crystal structure, provide a useful model for understanding native pEtN binding and reaction [40].

The EtN moiety found in the active site of MCR-1 is stabilised by the side chain of N329, a water molecule, and pT285. A structural overlay of the EtN-bound and nonbound crystals reveals the H395 side chain to be rotated 50° to accommodate EtN (Figure 4D). In particular, the introduction of EtN changes the hydrogen-bonding network in the active site, emphasising its flexibility towards 'induced fit' and hinting at the existence of different catalytic states. This EtN-bound structure was used to produce a model of pEtN covalently bound to T285, as illustrated in Figure 4E [XX], wherein the terminal $-NH_3^+$ of the pEtN occupies a pocket that shows an obvious negative electrostatic potential, with the complementary electrostatic charges providing an attractive binding potential. This binding model is supported in the most recent literature by a crystal structure showing the noncovalent binding of pEtN to a T315A catalytic site mutant of ICR^{Mc}, a pEtN transferase from *Moraxella catarrhalis* that has intrinsic colistin resistance [37]. A full PE substrate-binding model is discussed further below.

Given that EtN is an analogue of the natural substrate (pEtN), its strength as a potential inhibitor was analysed. Inhibition studies find that EtN alone did not influence the growth of MCR-1-expressing *E. coli*, but, in the presence of 4 mg/L polymyxin B, EtN concentration-dependent growth inhibition was seen over a concentration range of 0–10 mM [40]. An additional *in vitro* TLC experiment demonstrated that, upon addition of EtN, MCR-1 lost its ability to cleave pEtN from a fluorescently labelled substrate [40]. Although the dissociation constant (K_D) of EtN binding to MCR-1 is estimated to be ~600 mM, the findings outlined above suggest that EtN could serve as a useful lead for inhibitor development.

Mechanistic insights into MCR-1 function

Despite the growing evidence for MCR-1 being a pEtN transferase belonging to the alkaline phosphatase superfamily, the catalytic mechanism of pEtN transfer is poorly characterised to date. To provide mechanistic insights into MCR-1 function beyond the superposition of X-ray crystal structure analysis, Hinchliffe *et al.* used the computational technique of density functional theory (DFT) to generate a series of models of possible transition states along the pEtN transfer pathway [31]. This was explored with both mono- and di-zinc forms of the MCR-1 active site to identify the most likely zinc stoichiometry required for pEtN transfer. The calculations required the simplification of the key substrates, PE and lipid A as $[P(O)O(OMe)_2]^-$ and $[P(O)(OMe)OO]^{2-}$, respectively.

In the mono-zinc model (**1**, Figure 4F), the activated E246 abstracts a proton from the hydroxyl side chain of T285 that simultaneously carries out nucleophilic attack on the phosphate centre of the zinc-coordinated PE (**2**, Figure 4F). The nucleophilic attack results in cleavage of the acyl side chain from PE, producing the T285 adduct (**3**, Figure 4F). The coordination geometry about the central zinc ion is maintained throughout the postulated mechanistic pathway. E246 and D465 are isoenergetic and also geometrically accessible from T285, suggesting that both residues are capable of initiating the reaction pathway through proton abstraction from T285. By contrast, in the di-zinc model, T285 activation by D465 leads to a significant structural change and causes dissociation of T285 from the zinc ion in contrast to the activation by E246. As a result, the relative potential energy of the di-zinc system is higher than that of the mono-zinc model.

Despite the considerable sensitivity of the solvation model and the constraints used, these initial calculations indicate that MCR-1 requires only a single zinc equivalent to catalyse the pEtN transfer pathway, this being the zinc-labelled Zn1 as discussed above and the only Zn conserved in all eight MCR-1 crystal structures. Using this platform, further computational exploration with in-depth analyses around substrate orientation, and including other interacting residues and hydrogen bonding networks, will help unlock the underlying mechanism of MCR-1.

Although these calculations do not consider the second phosphoryl transfer of pEtN to lipid A, it is compelling to think that a second zinc ion, for example Zn2 discussed in the crystallography sections above, might be involved in lipid A phosphate binding. Zn2 binding to the lipid A phosphate in a location immediately adjacent to Zn1 and the T285-pEtN adduct potentially brings reactive centres together and could also provide electronic polarisation to afford the lipid A phosphate an energetic pathway towards forming a phosphoester bond with the pEtN moiety (Figure 4E).

MCR-1 function: MIC assays

To reveal the intricacies of the pEtN transfer mechanism of MCR-1, a series of MIC assays coupled with site-directed mutagenesis, *in vitro* TLC assays, and mass spectrometry analyses were conducted. Immunoblot assays were performed alongside mutagenesis to ensure that the MCR-1 mutations did not cause any change in expression levels and cellular location. Taken together with the crystallographic structure studies, these highlight functionally significant details of MCR-1 that could serve as targets for structure-based inhibitor designs.

The role of zinc ions and disulfide bonds

All of the published crystal structures contain at least one zinc ion in common, validating MCR-1 as a zinc metalloprotein. The significance of zinc ions in MCR-1 function is revealed through the treatment of MCR-1-positive *E. coli* with 250 mg/ml EDTA, a strong metal chelator [31]. Chelators such as EDTA are known to sensitise the outer membrane of *E. coli* and other Gram-negative bacteria, increasing their susceptibility to colistin and other antibiotics that do not penetrate Gram-negative cells [44]. Nevertheless, there is a clear reduction in the inhibitory concentration of colistin (from 2 mg/ml to 0.25 mg/ml) that is attributed to a loss of MCR-1 activity.

The periplasmic dithiol-disulfide oxidoreductase (DsbA) is a disulfide-inducing enzyme that enhances the activity of *Nm*EptA, the *N. meningitidis* homologue of MCR-1 [45]. DsbA catalyses the oxidation of cysteine residues on a protein and enhances the formation of disulfide bonds. Co-expression of MCR-1 with DsbA affords an approximately twofold increase in the colistin MIC (8 mg/ml) compared with its negative control [31]. As discussed previously, the soluble domain of MCR-1 contains three disulfide linkages that stabilise loops. The enhanced formation of disulfides by DsbA might help open up the substrate entry pathway in MCR-1, leading to an overall higher activity and commensurately greater drug resistance.

Essential active site residues

The MCR-1 active site captures one or more zinc ions, coordinating these with core residues that are conserved among pEtN transferases. The essentiality of putative key residues in MCR-1 bioactivity was probed over several independent studies using site-directed mutagenesis coupled with MIC assays. Despite some discrepancies arising from differences in protocols, bacterial strains, and vectors, the results are in general agreement, with the modification of five residues, E246, T285, D465, H466, and H478, greatly ablating polymyxin resistance in MCR-1-expressing cells.

Stojanoski *et al.* showed that the T285A variant reduces both colistin and polymyxin B MIC levels from 8.0 and 6.0 mg/ml to 0.125 and 0.092 mg/ml, respectively, in essence abolishing polymyxin resistance to the level of control experiments [32].

Hinchliffe *et al.* tested variants of E246, T285, K333, H395, E468, and H478 [31]. The E246A, T285A, and H395A variants reduced colistin MIC levels to the control level; the K333A, E468A, and H478A variants, although not abolishing MCR-1 activity, showed a significant reduction in the colistin MIC.

Wei *et al.* probed another set of variants, E246, T285, N329, K333, H395, D465, H466, and H478 [40]. In their experiments, only the H466A variant completely re-established polymyxin B antibacterial action. K333A and D465A variants only slightly ablated MCR-1 induced polymyxin B resistance; the remaining five variants significantly reduced the polymyxin B MIC, close to the level of control experiments.

Xu *et al.* assessed E246, T285, H390, D465, and H464 locations [11]. All five variants reduced the colistin MIC levels to the control levels, removing all resistance effects.

Hu *et al.* tested E246, T285, D299, E300, N329, S330, H395, D465, H466, and H478 [38]. The E246A, T285A, D465A, H466A, and H478A variants reduced colistin MIC levels to the control level, whereas the D299A, E300A, N329A, and S330A variants did not appear to affect colistin resistance, leaving MCR-1 activity more or less fully intact. Notably, the H395A variant had no effect on colistin resistance, contradicting the three independent results from the other groups, which saw significant or complete reduction in either polymyxin B or colistin resistance.

A summary of the MIC assays on all of the residues described above is provided in Table 1 and includes vector and bacterial strain details.

Phosphatidylethanolamine binding pocket

The natural substrate PE is a relatively large molecule with two acyl chains and serves as the source of pEtN abstracted by MCR-1. To date, there is no experimental evidence that demonstrates MCR-1 binding to PE. Although molecular docking of a PE molecule into MCR-1 coordinates proved impossible, Xu *et al.* docked PE into the homologous *Nm*EptA structure [11]. A superposition of the docked *Nm*EptA and MCR-1 structures revealed the putative PE binding pocket in MCR-1 that appears to be formed across both the transmembrane domain (magenta, Figure 3B) and the two periplasmic-facing helices (orange, Figure 3B). In the model, the phosphate group of PE binds to Zn1 and the NH_3^+ moiety of PE is buried in the active site pocket with its electronegative potential providing an attractive force. This was also demonstrated by the modelled T285-pEtN (Figure 4E). In addition to the five active site residues (E246, T285, H390, D465, and H466), Xu *et al.* identified the following seven residues positioned along the substrate entry pathway and assayed for their functional importance: N108, T112, E116, S330, K333, H395, and H478. Protein variants of the seven residues were tested by *in vitro* enzymatic assays, colistin susceptibility tests (Luria broth agar plate and broth dilution MIC assays), and matrix-assisted laser desorption/ionisation-time of flight (MALDI-TOF) mass spectrometry analysis.

The results indicated that the N108A, T112A, and S330A variants maintained partial colistin resistance, whereas the E116A variation completely abolished MCR-1 activity. Notably, T112 and E116 are the residues on the periplasmic-facing helices, PH2′ and PH2, respectively, that the modelling suggests are responsible for the recognition and engagement of the PE substrate. The K333A variant completely ablated colistin resistance, but this contradicts two earlier studies where partial MCR-1 activity was maintained. Variation at H395 also completely removed colistin resistance, supporting the findings of most of the other research groups. Finally, H478 was proven to be essential for MCR-1 activity, which is in agreement with point-mutation studies by all other groups.

A summary of the MIC assays of the above mutants is provided in Table 1.

Lipid A-binding pocket

Lipid A is the basal compartment of LPS that is modified with pEtN by MCR-1, yet the underlying molecular mechanism is poorly understood. No crystal structures of lipid A-bound MCR-1 are reported and this might be because of the lack of the transmembrane domain, the periplasmic face of which is implicated in the correct binding of the incoming substrates such as lipid A. Nevertheless, the currently available soluble domain crystal structures might hint at a putative lipid A-binding site located in close proximity to the active site [40]. Molecules of D-sorbitol [32], glycerol [31], D-glucose [40], and D-xylose [46], all of which bind in this putative lipid A pocket in the same orientation, form hydrogen bonds with three residues of T283, S284, and N482, the first two of which are conserved in MCR-1 homologues (Figure 5). The disaccharide backbone of lipid A comprises two glucosamine units, which are thought to be mimicked in part by these ligands.

In the case of D-glucose, the ligand is also flanked by Y287 and P481 in the putative lipid A pocket (residues not shown in Figure 5). A site-directed mutagenesis study of five residues in the putative pocket showed that P481A and Y287A variants in particular, impair MCR-1 function [40]. A summary of the MIC assays of the five lipid A pocket variants is provided in Table 1.

Although D-glucose itself does not affect polymyxin B resistance in binding MCR-1, this molecule might serve as a template for structure-based design of potential inhibitors. For example, positions 4 and 5 of the glucose ring that do not interact with any residues could be modified to probe novel binding interactions and provide inhibitory effects.

Concluding remarks and future perspectives

The recent reports of *mcr1* as a mobile colistin resistance gene in animal and human pathogens is a serious threat, further fuelling the current antibiotic resistance crisis [47,48]. To date, 11 new genetic variants of *mcr1* have been discovered across different countries, hinting at the possibility of an ongoing evolution and ever-changing target [49–51].

MCR-1 is a pEtN transferase encoded by *mcr1* that renders polymyxin antibiotics ineffectual. Although some mechanistic insights into the pEtN transfer reaction catalysed by MCR-1 are known and are highlighted in this review, limited knowledge of the physiological function, enzymatic mechanism, and the lack of full-length and PE- or lipid A-liganded crystal structures, calls for further investigations with the aim of targeting MCR-1 and/or other pEtN transferases with molecular inhibitors. The collective results presented in this review highlight functionally important regions and residues of MCR-1, and link site-directed mutagenesis and activity/inhibitory assays with 3D X-ray crystallographic coordinates. In particular, substrate mimetics EtN and D-glucose might serve as useful starting points for the rational drug design of molecular inhibitors of MCR-1 to use in colistin-based combination therapies, similarly to the example of the clavulanic acid/ß-lactam antibiotic combinations. Given that MCR-1 is structurally similar to other chromosomally encoded lipid A pEtN transferases, the design of MCR-1 inhibitors should also consider these other enzymes as potential targets. Broad-spectrum inhibitors acting collectively against bacterial pEtN transferases could afford a novel antimicrobial strategy by undermining membrane integrity, which might be more significant than combating polymyxin resistance specifically.

Acknowledgments

We thank the University of Auckland for a Doctoral Scholarship (R.H) and the Faculty of Science Faculty Research Development Fund (FRDF) for a Post-Doctoral Fellowship (S.J.S.).

References

1 Lim, L.M. *et al.* (2010) Resurgence of colistin: a review of resistance, toxicity, pharmacodynamics, and dosing. *Pharmacotherapy* 30, 1279–1291

2 Sekyere, O.J. *et al.* (2016) Colistin and tigecycline resistance in carbapenemase-producing Gram-negative bacteria: emerging resistance mechanisms and detection methods. *J. Appl. Microbiol.* 121, 601–617

3 Brink, A.J. *et al.* (2013) Emergence of OXA-48 and OXA-181 carbapenemases among *Enterobacteriaceae* in South Africa and evidence of *in vivo* selection of colistin resistance as a consequence of selective decontamination of the gastrointestinal tract. *J. Clin. Microbiol.* 51, 369–372

4 Rodriguez-Avial, C. *et al.* (2012) *Klebsiella pneumoniae*: development of a mixed population of carbapenem and tigecycline resistance during antimicrobial therapy in a kidney transplant patient. *Clin. Microbiol. Infect.* 18, 61–66

5 Liu, Y-Y. *et al.* (2016) Emergence of plasmid-mediated colistin resistance mechanism MCR-1 in animals and human beings in China: a microbiological and molecular biological study. *Lancet Infect. Dis.* 16, 161–168

6 WHO Advisory Group on Integrated Surveillance of Antimicrobial Resistance (2017) *Critically Important Antimicrobials for Human Medicine – 5th Revision,* WHO

7 Al-Tawfiq, J.A. *et al.* (2017) How should we respond to the emergence of plasmid-mediated colistin resistance in humans and animals? *Int. J. Infect. Dis.* 54, 77–84

8 Xavier, B.B. *et al.* (2016) Identification of a novel plasmid-mediated colistin-resistance gene, *mcr-2* in *Escherichia coli. Eurosurveillance* 21, 30280

9 Yin, W. *et al.* (2017) Novel plasmid-mediated colistin resistance gene *mcr-3* in *Escherichia coli. mBio* 8, e00543-17

10 Borowiak, M. *et al.* (2017) Identification of a novel transposon-associated phosphoethanolamine transferase gene, *mcr-5*, conferring colistin resistance in *d*-tartrate fermenting *Salmonella enterica* subsp. *enterica serovar Paratyphi B. J. Antimicrob. Chemother.* 72, 3317–3324

11 Xu, Y. *et al.* (2018) Mechanistic insights into transferable polymyxin resistance among gut bacteria. *J. Biol. Chem.* 293, 4350–4365

12 Hancock, R.E.W. and Chapple, D. S. (1997) Peptide antibiotics. *Antimicrob. Agents Chemother.* 43, 1317–1323

13 Falagas, M.E. *et al.* (2010) Resistance to polymyxins: mechanisms frequency and treatment options. *Drug Resist. Updat.* 13, 132–138

14 Li, J. *et al.* (2006) Colistin: the re-emerging antibiotic for multidrug-resistant Gram-negative bacterial infections. *Lancet Infect. Dis.* 6, 589–601

15 Poirel, L. *et al.* (2017) Polymyxins: antibacterial activity, susceptibility testing, and resistance mechanisms encoded by plasmids or chromosomes. *Clin. Microbiol. Rev.* 30, 557–596

16 Dixon, R.A. and Chopra, I. (1986) Leakage of periplasmic proteins from *Escherichia coli* mediated by polymyxin B nonapeptide. *Antimicrob. Agents Chemother.* 29, 781–788

17 Powers, J.P. and Hancock, R. E. (2003) The relationship between peptide structure and antibacterial activity. *Peptides* 24, 1681–1691

18 Pristovšek, P. and Kidrič, J. (2004) The search for molecular determinants of LPS inhibition by proteins and peptides. *Curr. Top. Med. Chem.* 4, 1185–1201

19 Velkov, T. *et al.* (2010) Structure-activity relationships of polymyxin antibiotics. *J. Med. Chem.* 53, 1898–1916

20 Zhou, Z. *et al.* (2001) Lipid A modifications in polymyxin-resistant *Salmonella typhimurium*: PMRA-dependent 4-amino-4deoxy-L-arabinose, and phosphoethanolamine incorporation. *J. Biol. Chem.* 276, 43111–43121

21 Lee, H. *et al.* (2004) The PmrA-regulated pmrC gene mediates phosphoethanolamine modification of lipid A and polymyxin resistance in *Salmonella enterica*. *J. Bacteriol.* 186, 4124–4133

22 Trent, M.S. *et al.* (2001) An inner membrane enzyme in *Salmonella* and *Escherichia coli* that transfers 4-amino-4-deoxy-L-arabinose to lipid A: induction on polymyxin-resistant mutants and role of a novel lipid-linked donor. *J. Biol. Chem.* 276, 43122–43131

23 Hankins, J.V. *et al.* (2012) Amino acid addition to *Vibrio cholerae* LPS establishes a link between surface remodeling in Gram-positive and Gram-negative bacteria. *Proc. Natl. Acad. Sci. U. S. A.* 109, 8722–8727

24 Trombley, M.P. *et al.* (2015) Phosphoethanolamine transferase LptA in *Haemophilus ducreyi* modifies lipid A and contributes to human defensin resistance *in vitro*. *PLoS One* 10, e0124373

25 Naessan, C.L. *et al.* (2008) Genetic and functional analysis of PptA a phospho-form transferase targeting type IBV pili in *Neisseria gonorrhoeae*. *J. Bacteriol.* 190, 387–400

26 Young, N.M. *et al.* (2013) Review of phosphocholine substituents on bacterial pathogen glycans: synthesis, structures and interactions with host proteins. *Mol. Immunol.* 56, 563–573

27 Cullen, T.W. *et al.* (2012) Characterization of unique modification of flagellar rod protein FlgG by *Campylobacter jejuni* lipid A phosphoethanolamine transferase, linking bacterial locomotion and antimicrobial peptide resistance. *J. Biol. Chem.* 287, 3326–3336

28 Cullen, T.W. *et al.* (2013) EptC of *Campylobacter jejuni* mediates phenotypes involved in host interactions and virulence. *Infect. Immun.* 81, 430–440

29 Aas, F.E. *et al.* (2006) *Neisseria gonorrhoeae* type IV pili undergo multisite, hierarchical modifications with phosphoethanolamine and phosphocholine requiring an enzyme structurally related to lipopolysaccharide phosphoethanolamine transferases. *J. Biol. Chem.* 281, 27712–27723

30 Kim, E.E. and Wyckoff, H. W. (1991) Reaction mechanism of alkaline phosphatase based on crystal structures. *J. Mol. Biol.* 218, 449–464

31 Hinchliffe, P. *et al.* (2017) Insights into the mechanistic basis of plasmid-mediated colistin resistance from crystal structures of the catalytic domain of MCR-1. *Sci. Rep.* 7, 39392

32 Stojanoski, V. *et al.* (2016) Structure of the catalytic domain of the colistin resistance enzyme MCR-1. *BMC Biol.* 14, 81

33 Cullen, T.W. and Trent, M.S. (2010) A link between the assembly of flagella and lipooligosaccharide of the Gram-negative bacterium *Campylobacter jejuni*. *Proc. Natl. Acad. Sci. U. S. A.*, 107, 5160–5165

34 Scott, N.E. *et al.* (2012) Modification of the *Campylobacter jejuni N*-linked glycan by EptC protein-mediated addition of phosphoethanolamine. *J. Biol. Chem.* 287, 29384–29396

35 Fage, C.D. *et al.* (2014) Crystallographic study of the phosphoethanolamine transferase EptC required for polymyxin resistance and motility in *Campylobacter jejuni*. *Acta Crystallogr. D* D70, 2730–2739

36 Ma, G. *et al.* (2016) High resolution crystal structure of the catalytic domain of MCR-1. *Sci. Rep.* 6, 39540

37 Stogios, P.J. *et al.* (2018) Substrate recognition by a colistin resistance enzyme from *Moraxella catarrhalis*. *ACS Chem. Biol.* 13, 1322–1332

38 Hu, M. *et al.* (2016) Crystal structure of *Escherichia coli* originated MCR-1, a phosphoethanolamine transferase for colistin resistance. *Sci. Rep.* 6, 38793

39 Cox, A.D. *et al.* (2003) Phosphorylation of the lipid A region of meningococcal lipopolysaccharide: identification of a family of transferases that add phosphoethanolamine to lipopolysaccharide. *J. Bacteriol.* 185, 3270–3277

40 Wei, P. *et al.* (2018) Substrate analog interaction with MCR-1 offers insight into the rising threat of the plasmid-mediated transferable colistin resistance. *FASEB J.* 32, 1085–1098

41 Anandan, A. *et al.* (2017) Structure of a lipid A phosphoethanolamine transferase suggests how conformational changes govern substrate binding. *Proc. Natl. Acad. Sci. U. S. A.* 114, 2218–2223

42 Ulmschneider, M.B. and Sansom, M.S. (2001) Amino acid distributions in integral membrane protein structures. *Biochim. Biophys. Acta.* 1512, 1–14

43 Wanty, C. *et al.* (2013) The structure of the neisserial lipooligosaccharide phosphoethanolamine transferase (LptA) required for resistance to polymyxin. *J. Mol. Biol.* 425, 3389–3402

44 Vaara, M. (1992) Agents that increase the permeability of the outer membrane. *Microbiol. Rev.* 56, 395–411

45 Piek, S. *et al.* (2014) The role of oxidoreductases in determining the function of the neisserial lipid A phosphoethanolamine transferase required for resistance to polymyxin. *PLoS One* 9, e106513

46 Liu, Z-X. *et al.* (2018) Crystal structure of the catalytic domain of MCR-1 (cMCR-1) in complex with D-xylose. *Crystals* 8, 172

47 Shen, Z. *et al.* (2016) Early emergence of *mcr-1* in *Escherichia coli* from food-producing animals. *Lancet Infect. Dis.* 16, 293

48 Zhou, H.-W. *et al.* (2017) Occurrence of plasmid- and chromosome-carried *mcr–1* in waterborne *Enterobacteriaceae* in China. *Antimicrob. Agents Chemother.* 61, e00017

49 Di Pilato, V. *et al.* (2016) *Mcr-1.2,* a new mcr variant carried on a transferable plasmid from a colistin-resistant KPC carbapenemase-producing *Klebsiella pneumoniae* strain of sequence type 512. *Antimicrob. Agents Chemother.* 60, 5612–5615

50 Sun, J. *et al.* (2018) Towards understanding MCR-like colistin resistance. *Trends Microbiol.* Published online March 7, 2018. https://dx.doi.org/10.1016/j.tim.2018.02.006

51 Yang, Y.Q. *et al.* (2017) Colistin resistance gene *mcr-1* and its variant in *Escherichia coli* isolates from chickens in China. *Antimicrob. Agents Chemother.* 61, e01204-16

Figure 1. Polymyxin mechanism of action in the presence or absence of mobile colistin resistance 1 (MCR-1): (a) The positively charged polymyxin heads are electrostatically attracted to the negatively charged lipid A moieties of lipopolysaccharides (LPS); (b) MCR-1 decorates lipid A of LPS with phosphoethanolamine (pEtN), which neutralises the overall negative charge. The positively charged polymyxin heads are no longer attracted to the pEtN-decorated LPSs.

Figure 2. Proposed mechanism of mobile colistin resistance 1 (MCR-1) action. The catalytic domain of MCR-1, a transmembrane protein expressed in the inner membrane, decorates Kdo2-lipid A with a phosphoethanolamine (pEtN) moiety. The pEtN moiety is abstracted from phosphatidylethanolamine (PE), a phospholipid substrate that is heavily localised in the inner membrane. The modified pEtN-Kdo2-lipid A is subsequently exported and presented in the outer membrane.

Figure 3. The structure of mobile colistin resistance 1 (MCR-1), including a transmembrane (TM) domain modelled from a crystal structure of the *Nm*EptA homolog [41]: (a) Secondary structure, domain, and topology model of MCR-1 [11,41]. The nomenclature can differ between published structures for the soluble periplasmic domain; (b) Full-length model of MCR-1 produced from crystal structure and homology models [11,41]; (c) Two views (rotated by 90°) of the MCR-1 soluble domain highlighting the large, slightly concave membrane-interacting surface. The active site is marked by a black box; (d) Surface diagrams viewed in the same orientation as (c), right. Left: colours are mapped by hydrophobicity (red, hydrophobic; white, hydrophilic). Right: colours are mapped by electrostatic potential (red, negative potential; white, neutral; blue, positive potential).

Figure 4. Mobile colistin resistance 1 (MCR-1) active site structures showing zinc ethanolamine (EtN)/phosphoethanolamine (pEtN) coordination, and the postulated phosphorylation pathway: (a) Structure 5LRM by Hinchliffe *et al.*, a representative model of the native T285 active site structure, displays a tetrahedral geometry around each zinc ion [31]. Asterisks denote residues from a symmetry-related molecule; (b) 5LRN by Hinchliffe *et al.,* a representative model of the pT285 active site structure coordinated by a single zinc ion [31]; (c) 5K4P by Stojanoski *et al.,* a representative model of the pT285 active site structure coordinated by four zinc ions. Asterisks denote zinc ion/residues from a symmetry-related molecule [32]; (d) Overlay of EtN-soaked (yellow) and nonsoaked (cyan) crystal structures; (e) model of T285-pEtN interacting with both Zn1 and Zn2 (top). Surface diagram of the active site accommodating the modelled T285-pEtN showing the negative (red) electrostatic potential of the active site pocket (bottom) [40]. The model suggests that Zn2, as a surface exposed feature, interacts with a phosphate from the second substrate (lipid A), both polarising the incoming phosphate and orienting lipid A appropriately for the second pEtN transfer; (f) Postulated phosphorylation pathway of a single zinc-containing MCR-1 active site modelled through density functional theory calculation [31].

Figure 5. Putative lipid A-binding pocket accommodating different ligand mimetics: (a) D-sorbitol from 5K4P [32]; (b) glycerol from 5LRN [31]; and (c) D-glucose from 5YLF [40]. D-Xylose from 5ZJV (not shown) is oriented in a similar manner to D-glucose [46].

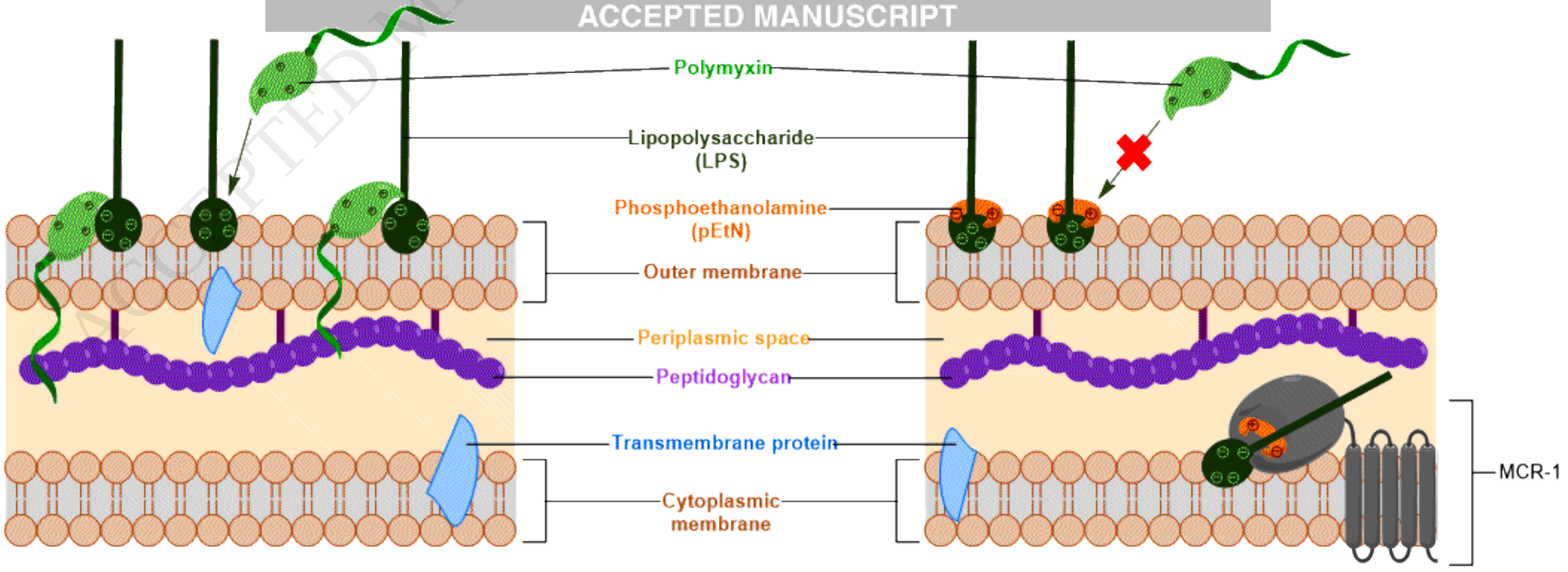

(A) Polymyxin binds to LPS in the absence of MCR-1

(B) Polymyxin cannot bind LPS in the presence of MCR-1

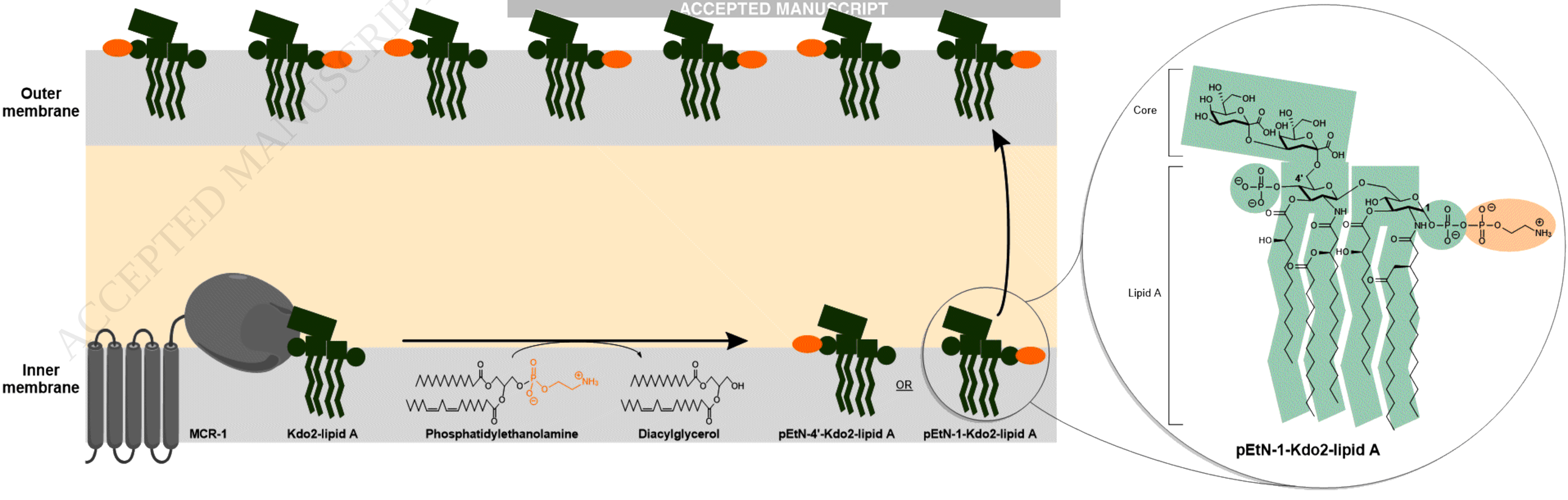

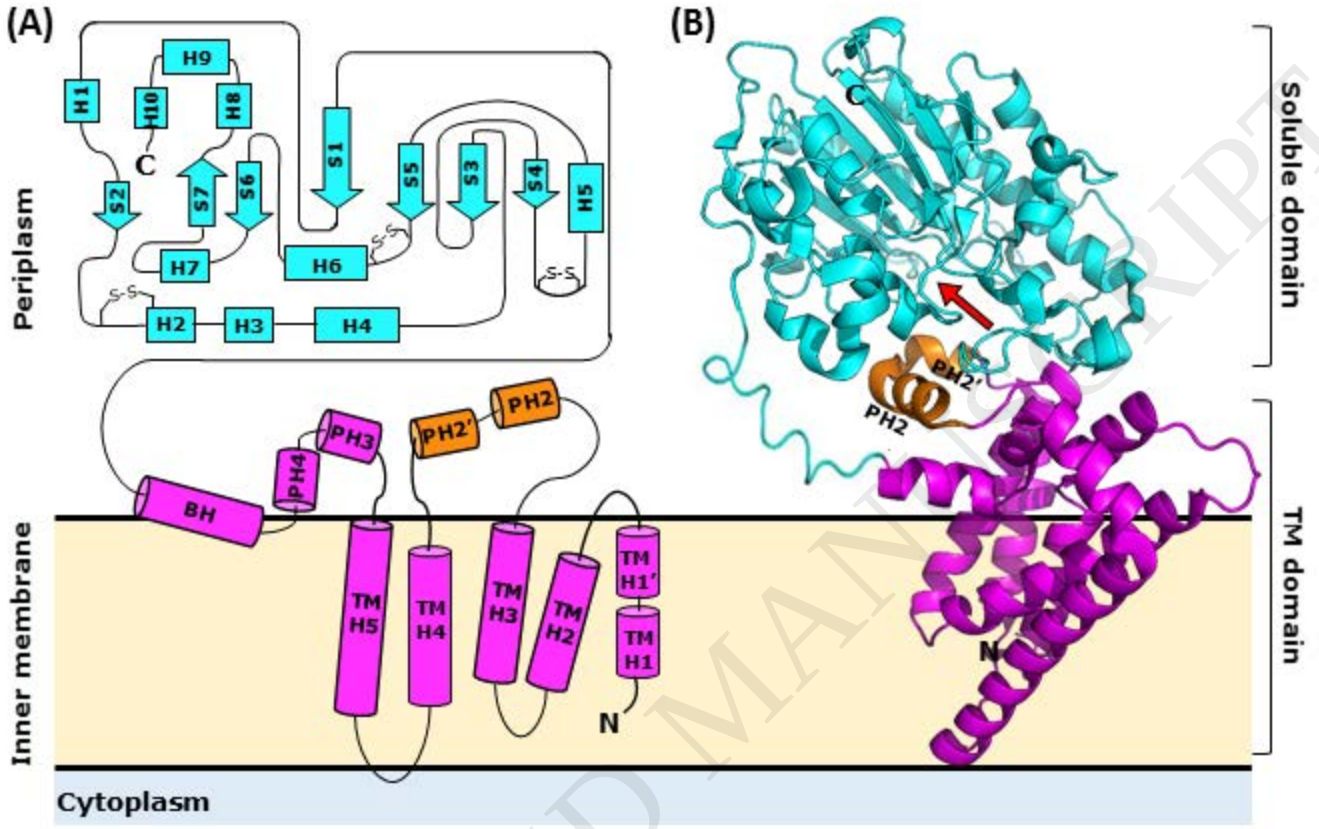

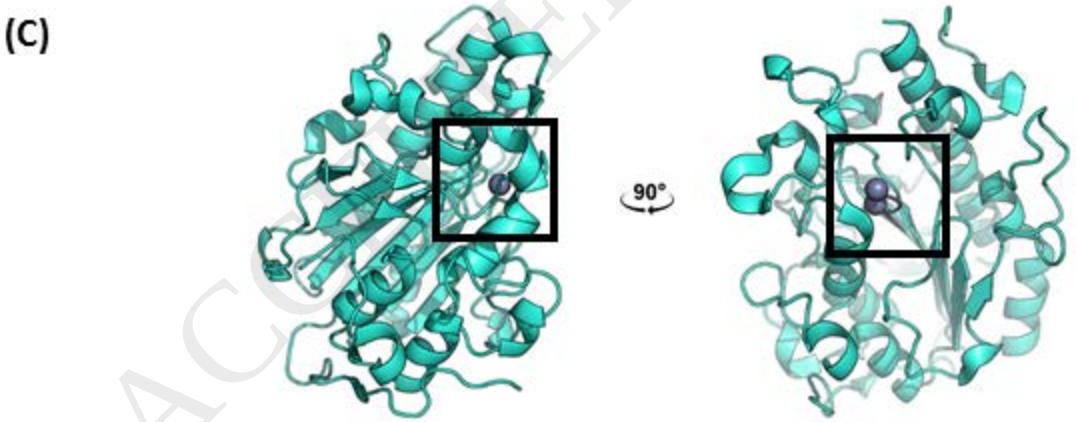

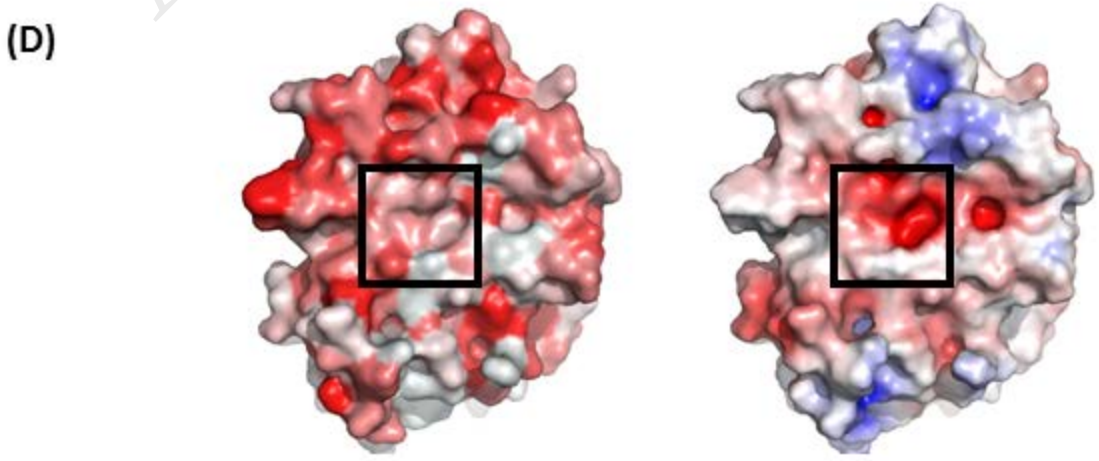

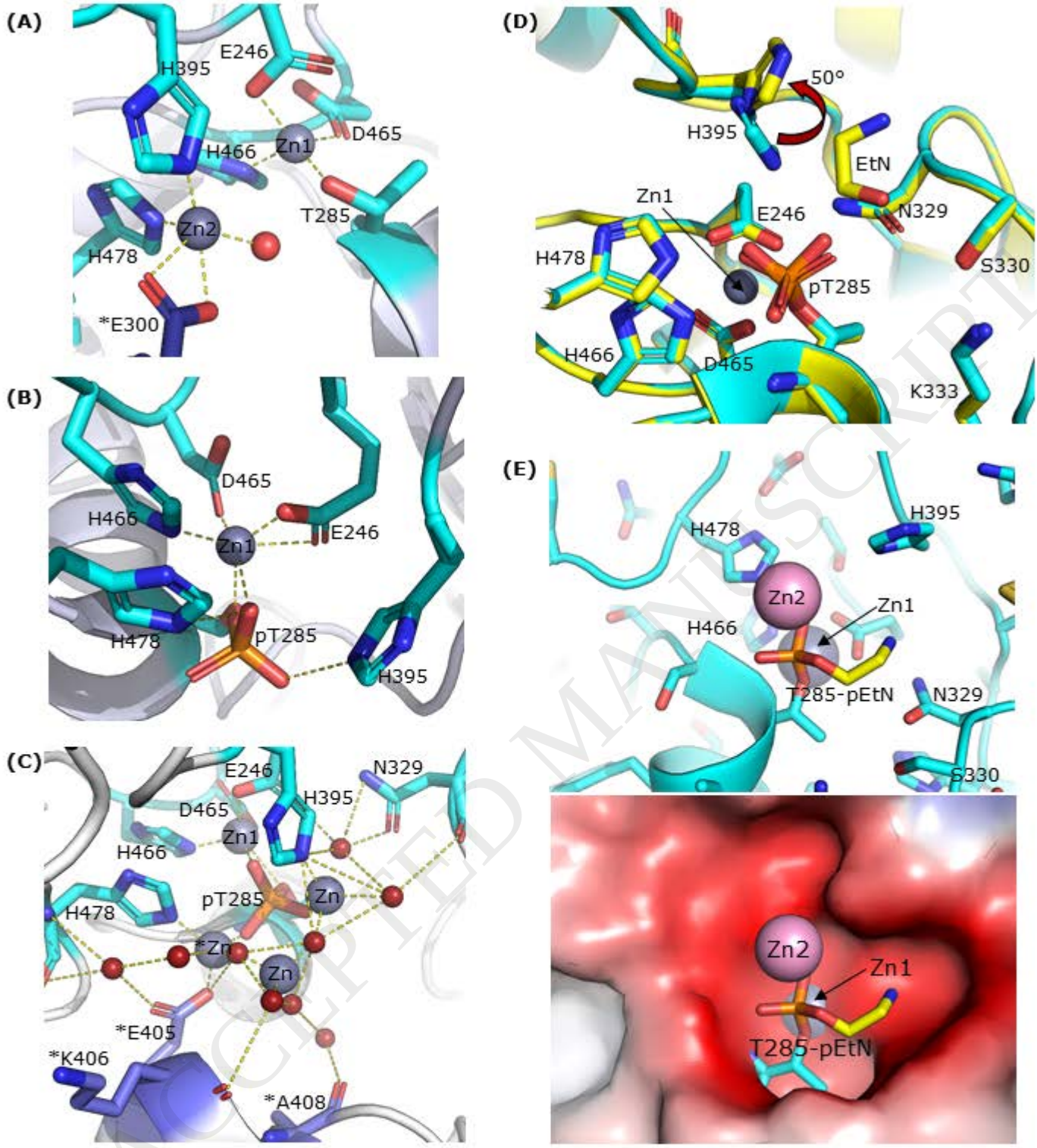

(F)

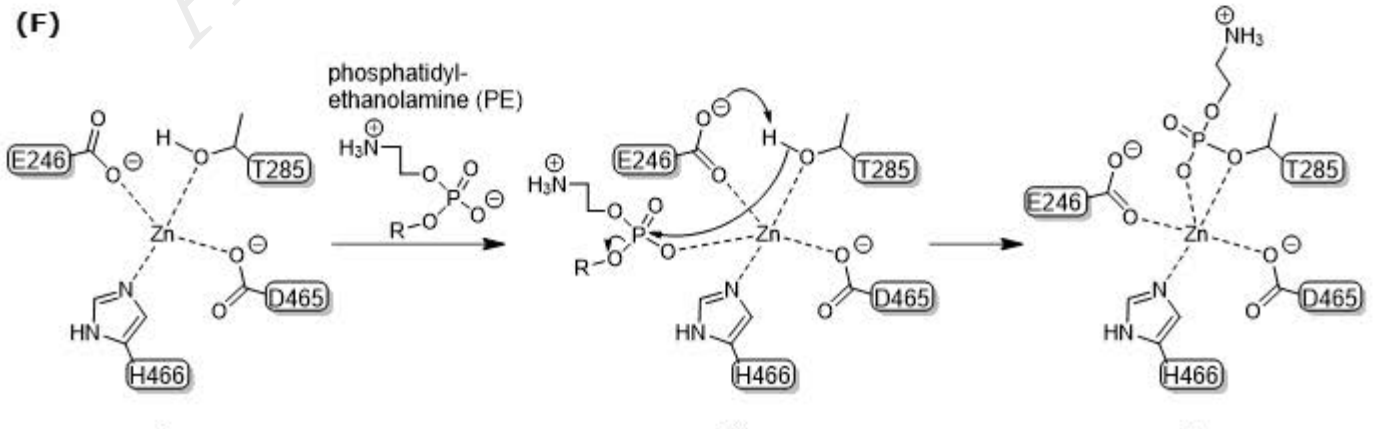

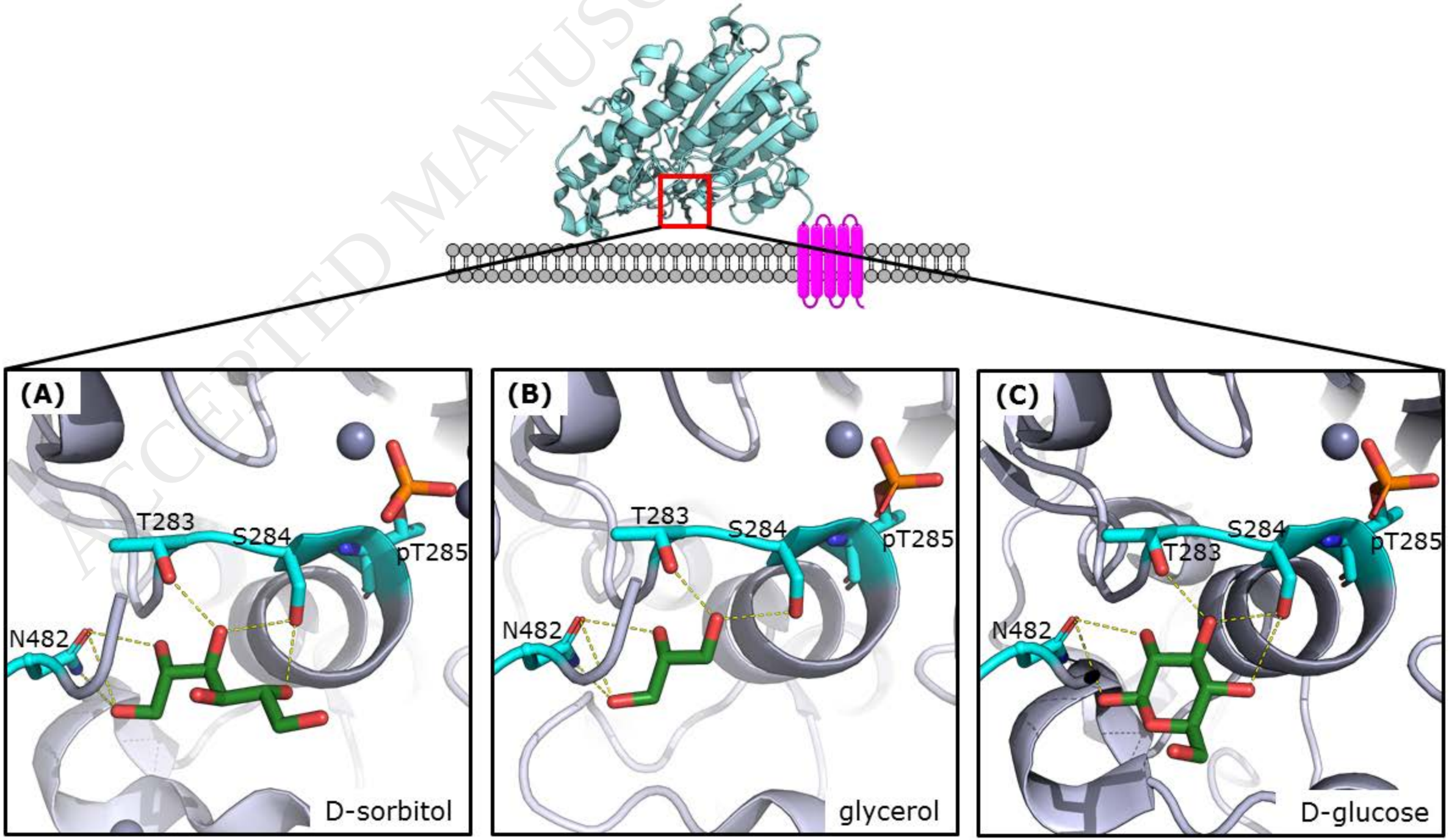

Table 1. Summary of MIC assays performed on MCR-1 variants[a]

MIC (mg/ml)								Experimental parameters			Refs
Negative control	Wild type	MCR-1 residue						Antibiotics used	Vector	Strain	
Residues in active site											
		E246A	T285A	H395A	D465A	H466A	H478A				
Binding		Zn1	Zn1, phosphorylation	Zn2, phosphate	Zn1	Zn1	Zn2, phosphate				
0.25	*4.0*	*0.25*	*0.25*	*0.25*	*0.25*	*0.25*	*0.25*	*Colistin*	*pBAD24*	*Escherichia coli MG1655*	*[11]*
1–2	*8–16*	*2–4*	*2–4*	*2–4*	*4–8*	*1–2*	*2–4*	*Polymyxin B*	*pET-28a(+)*	*E. coli Rosetta*	*[40]*
2.0	*8.0*	*2.0*	*2.0*	*8.0*	*2.0*	*2.0*	*2.0*	*Colistin*	*pET-15b*	*E. coli BL21*	*[38]*
0.032	*6.0*		*0.092*					*Polymyxin B*	*pET-28a*	*E. coli BL21(DE3)*	*[32]*
0.032	*8.0*		*0.125*					*Colistin*	*pET-28a*	*E. coli BL21(DE3)*	*[32]*
≤0.125	*4.0*	*≤0.125*	*≤0.125*	*≤0.125*			*0.5*	*Colistin*	*pUC19*	*E. coli TOP10*	*[31]*
Other residues within 20 Å of active site											
		D299A	E300A	N329A	H390A	E468A					
0.25	*4.0*				*0.25*			*Colistin*	*pBAD24*	*E. coli MG1655*	*[11]*
1–2	*8–16*			*2–4*				*Polymyxin B*	*pET-28a(+)*	*E. coli Rosetta*	*[40]*
2.0	*8.0*	*8.0*	*8.0*	*8.0*				*Colistin*	*pET-15b*	*E. coli BL21*	*[38]*
≤0.125	*4.0*					*0.25*		*Colistin*	*pUC19*	*E. coli TOP10*	*[31]*
Residues within 15 Å of active site (putative PE substrate pocket)											
		N108A	T112A	E116A	S330A	K333A					
0.25	*4.0*	*2.0*	*0.5*	*0.25*	*2.0*	*0.25*		*Colistin*	*pBAD24*	*E. coli MG1655*	*[11]*
1–2	*8–16*					*4–8*		*Polymyxin B*	*pET-28a(+)*	*E. coli Rosetta*	*[40]*
2.0	*8.0*				*8.0*			*Colistin*	*pET-15b*	*E. coli BL21*	*[38]*
0.125	*4.0*					*0.25*		*Colistin*	*pUC19*	*E. coli TOP10*	*[31]*
Residues in putative lipid A-binding pocket											
		T283A	S284A	Y287A	P481A	N482A					
1–2	*8–16*	*8–16*	*8–16*	*2–4*	*4–8*	*8–16*		*Polymyxin B*	*pET-28a(+)*	*E. coli Rosetta*	*[40]*

[a] *Yellow-highlighted MIC values denote complete ablation of MCR-1-associated drug resistance.*